Available online at BCREC website: https://bcrec.id

Bulletin of Chemical Reaction Engineering & Catalysis, 18 (1) 2023, 71-84

Research Article

Preparation of Au/ZnO/Fe_3O_4 Composite for Degradation of Tartrazine under Visible Light

Linh Vo Quang, Anh-Tuan Vu*

School of Chemical Engineering, Hanoi University of Science and Technology, Vietnam.

Received: 6th January 2023; Revised: 17th February 2023; Accepted: 18th February 2023
Available online: 20th February 2023; Published regularly: March 2023

Abstract

Zinc oxide has been shown to be a potential photocatalyst under UV light but its catalytic activity is limited under visible light due to its wide bandgap energy and rapid recombination of electrons and holes. Besides the catalytic recovery is a challenging issue because of its dispersion in solution. Previous work has shown that the interaction of gold nanoparticles with ZnO can reduce the band gap energy (E_g) and plasmon resonance (SPR) as well as the formation of the Schottky barrier in Au/ZnO composite can reduce the recombination of electrons and holes. In this study, Au/ZnO/Fe_3O_4 (AZF) composites were prepared by a simple mixing method using polyvinyl alcohol (PVA) as a binder. As-prepared composites were characterized by Scanning Electron Microscope (SEM), Energy Dispersive X-ray Spectroscopy (EDS), X-ray Diffraction (XRD), UV-Vis Diffuse Reflectance (UV-Vis-DR), and Fourier Transform Infra Red (FT-IR). The catalytic efficiency of as-prepared samples was evaluated through the decomposition of tartrazine (TA), a colorant that is difficult to decompose in wastewater and has harmful effects on human health. The effects of reaction parameters such as the content of PVA, solution pH, and oxidizing agents (O_2 and H_2O_2) on the catalytic efficiency were studied. The AZF at PVA of 0.0125 g showed the highest performance among as-prepared samples. With the presence of 12 mM H_2O_2 in the catalyst system, the degradation efficiency and reaction rate of TA in composite increased to 81.5% and 0.020 min^{-1}, respectively. At this condition, photocatalysis and Fenton system catalysis occurred together. The catalytic mechanism of Tartrazine (TA) on composite was proposed and the reaction of TA was studied by the first-order kinetic model.

Copyright © 2023 by Authors, Published by BCREC Group. This is an open access article under the CC BY-SA License (https://creativecommons.org/licenses/by-sa/4.0).

Keywords: Composite; Degradation; Photocatalyst; Tartrazine; Fenton catalyst

How to Cite: L.V. Quang, A.-T. Vu (2023). Preparation of Au/ZnO/Fe_3O_4 Composite for Degradation of Tartrazine under Visible Light. *Bulletin of Chemical Reaction Engineering & Catalysis*, 18(1), 71-84 (doi: 10.9767/bcrec.17061)

Permalink/DOI: https://doi.org/10.9767/bcrec.17061

1. Introduction

In light of rapid industrialization along with population growth, water pollution is becoming a hot issue in all countries in the world. Accordingly, industrial wastes discharge into water often containing organic and inorganic matter including heavy metals, synthetic organic dyes, pesticides, and petroleum hydrocarbons not only cause serious effects on health humans or organisms but also pose a serious threat to environmental sustainability [1]. This is going to be a challenge for the development of a country's industry and economy. Therefore, global researchers have focused on developing methods to treat pollution. In this context, various processes and technologies based on adsorption, biological, and oxidation methods have been designed. Among these methods, the oxidation process for the degradation of organic compounds by oxygen and hydroperoxide in heterogeneous nanomaterials using sunlight has been widely researched, developed, and applied. Un-

* Corresponding Author.
Email: tuan.vuanh@hust.edu.vn (A.-T. Vu);
Cell phone: +84-912911902, Fax +84-0243 868 0070

der the irradiation of light, photoexcited charge carriers are turned into reactive oxygen species (ROS), for instance, superoxide radical anions ($\cdot O_2^-$) and hydroxyl radicals ($\cdot OH$), to mineralize poisonous organic compounds yielding CO_2 and H_2O species during the photodegradation process [1,2].

ZnO is one of the semiconductor oxides that has attracted the attention of scientists because of its popularity, low cost, and environmental friendliness. It can be used as an adsorbent, paint, and cosmetics [3–6]. However, in the field of photocatalysis, ZnO encounters limitations such as poor adsorption of sunlight due to high band gap energy and rapid recombination of electrons and holes. Therefore, it is necessary to look for methods to solve these problems to expand the application of ZnO [7]. There are several types of research on doping precious metals into ZnO to reduce band gap energy, increase visible light absorption, and lower electron and hole recombination. To solve this problem, the proposed solution is to dope an appropriate amount of precious metals such as Au, Ag, Pt, and Pb, which enhances sunlight absorption and reduces electron-hole recombination, resulting in increased decomposition of organic substances [7–15].

Commonly, ZnO-based composites are micro-materials and have very low density. Thus, it is challenging to remove composites from the solution after the catalytic process. This is a significant limitation for the reuse of catalysts. Fe_3O_4 magnetic nanomaterials as an alternative, differentiate other materials from aqueous solutions by external magnets. This separation helps to avoid the loss of solid catalysts in the process and is not time-consuming. It also enhances product purity and optimizes operating costs [16–19]. To combine composites with Fe_3O_4, a natural polymer or synthetic polymer can be used as a binder. Polyvinyl alcohol (PVA) is widely used in the adsorption process because of its nontoxicity, low cost, chemical stability, and many hydroxyl groups [20,21]. Therefore, an interesting proposal is to combine composites with Fe_3O_4 utilizing PVA.

According to our previous study, Au/ZnO composite at 5 wt% of Au had the best photocatalytic performance compared to other Au contents, the degradation efficiency for tartrazine approached 99.2% in 60 min [13]. However, Au/ZnO is very low density, it is difficult to recover Au/ZnO from the solution after the catalysis process. Besides, at the high cost of Au, the increase in Au content may lead to limitations in the practical application of the catalyst. Therefore, the idea is the combination of Au/ZnO and Fe_3O_4 magnetic materials with PVA binders to improve the recovery of contact by magnets after the reaction. Besides, Fe_3O_4 is also shown to be a Fenton catalyst in the presence of H_2O_2. Furthermore, photocatalysis and Fenton occur simultaneously and the effects of reaction conditions also need to be sufficiently studied. In this study, Au/ZnO/Fe_3O_4 composites were synthesized by simple mixing method. The catalytic efficiency of the as-prepared materials was evaluated by the decomposition of TA. The effects of material structure and PVA content on the degradation of TA were studied. In addition, the effects of the reaction conditions of the Fenton process and the oxidants (H_2O_2 and O_2) were evaluated under visible light. The recovery efficiency of nanocomposite materials was also of great interest through the reusability of the catalyst. Furthermore, the kinetics of the catalytic process was modeled according to the first-order kinetics equation.

2. Materials and Methods

2.1 Materials

Zinc nitrate hexahydrate ($Zn(NO_3)_2.6H_2O$, 99.5%), urea ($(NH_2)_2CO$, 99.5%), gold (III) chloride tetrahydrate ($HAuCl_4.4H_2O$, 99%), sodium citrate ($Na_3C_6H_5O_7$, 99%), iron (II) sulfate heptahydrate ($FeSO_4.7H_2O$, 99%), iron (III) chloride hexahydrate ($FeCl_3.6H_2O$, 99%), sodium hydroxide (NaOH, 96%), Polyvinyl alcohol (99.8%) were purchased from China, Tartrazine (99%) were obtained from Sigma-Aldrich.

2.2 Preparation of ZnO

The hydrothermal method was doped for the synthesis of the flower-like ZnO. Ordinarily, 4.4623 g of $Zn(NO_3)_2.6H_2O$ and 1.8018 g of urea were poured into 100 mL of distilled water under stirring for 30 min to form a transparent mixed solution. This solution mixture was transferred into Teflon-lined sealed stainless-steel autoclaves and kept in a hydrothermal oven at a temperature of 90 °C for 24 h. Then the beaker was taken outside and allowed to cool naturally to room temperature. The precipitate was filtered, washed with distilled water and ethanol a few times, and dried at 90°C for 24 h. Finally, the ZnO nanoflowers were obtained after calcinating the precipitate at 400 °C for 2 h with a heating rate of 2 °C/min. The formation of ZnO was described by the following Equations (1)-(5) [13]:

Copyright © 2023, ISSN 1978-2993

$$(NH_2)_2CO + 3H_2O \rightarrow 2NH_3.H_2O + CO_2 \quad (1)$$

$$NH_3.H_2O \rightarrow NH_4^+ + OH^- \quad (2)$$

$$CO_2 + OH^- \rightarrow CO_3^{2-} + H_2O \quad (3)$$

$$4Zn^{2+} + CO_3^{2-} + 6OH^- + H_2O \rightarrow Zn_4(CO_3)(OH)_6.H_2O \quad (4)$$

$$Zn_4(CO_3)(OH)_6.H_2O \rightarrow 4ZnO + CO_2 + 4H_2O \quad (5)$$

2.3 Synthesis of Au/ZnO Composite

Au/ZnO composites were facially fabricated by the reduction of acid chloroauric by sodium citrate, the synthesis procedure is shown in Figure 1. In the previous report, Au/ZnO composite at 5 wt% of Au had the best photocatalytic performance in the degradation of tartrazine compared to other Au contents [13]. Besides, at the high cost of Au, the increase in Au content may lead to limitations in the practical application of the catalyst. Therefore, in this study, 5 wt% Au was selected to prepare Au/ZnO. First, the desired volume of 0.005 M $HAuCl_4$ (at 5 wt% Au) and $Na_3C_6H_5O_7$ 1% solutions were stirred together for 5 min. An amount of 0.1 g of ZnO was added into the solution and sonicated for 5 min and then stirred for 1 h to obtain a purple precipitate. It was filtered and washed with distilled water and ethanol to remove impurity ions, and then dried at 80 °C in the air for 12 h to obtain Au/ZnO composite.

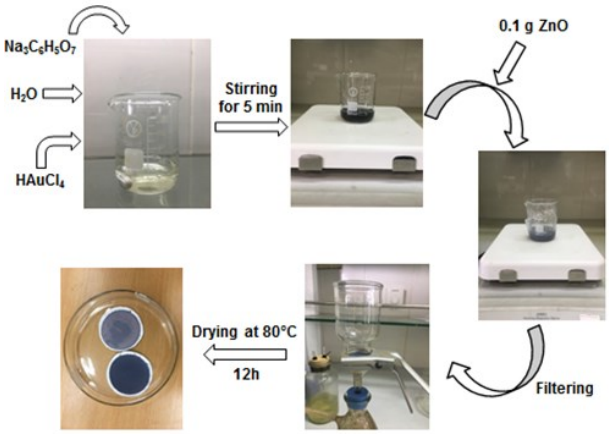

Figure 1. The synthesis procedure of Au/ZnO composite.

2.4 Synthesis of Fe_3O_4 Magnetic Nanoparticles

Fe_3O_4 magnetic nanoparticles (MNPs) were synthesized by a co-precipitation method. Normally, 1.078 g of $FeSO_4.7H_2O$ and 2.098 g of $FeCl_3.6H_2O$ were poured into 50 mL of distilled water under stirring to form a mixed solution. Next, NaOH 2M solution was added to the above solution using a peristaltic pump under constant magnetic stirring, and the final pH was 11. The above solution was heated at 60 °C and then stirred for 3 h. The resulting particles were magnetically separated and washed repeatedly with distilled water and ethanol until pH approached 7. Then dried at 80 °C in the air for 12 h. Finally, the Fe_3O_4 material was finely ground to obtain the black precipitate. The synthesis procedure of Fe_3O_4 and its magnetic properties are presented in Figure 2.

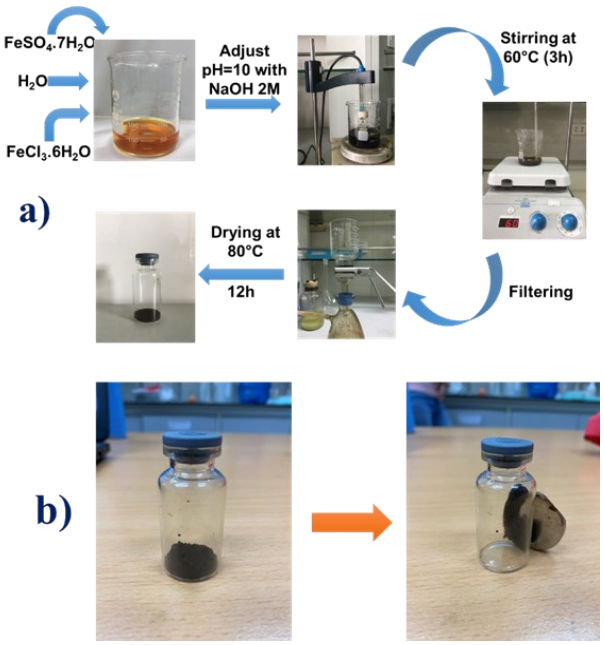

Figure 2. (a) The synthesis procedure of Fe_3O_4 and (b) Test the magnetism of Fe_3O_4 with a magnet.

$$Fe^{2+} + 2Fe^{3+} + 8OH^- \rightarrow Fe_3O_4 + 4\ H_2O \quad (6)$$

2.5 Preparation of AZF Nnanocomposite

0.1 g of Fe_3O_4 was ultrasonicated in 15 mL of distilled water until complete dispersion. And, a certain amount of PVA needed to be dissolved in 15 mL of distilled water at 90 °C for

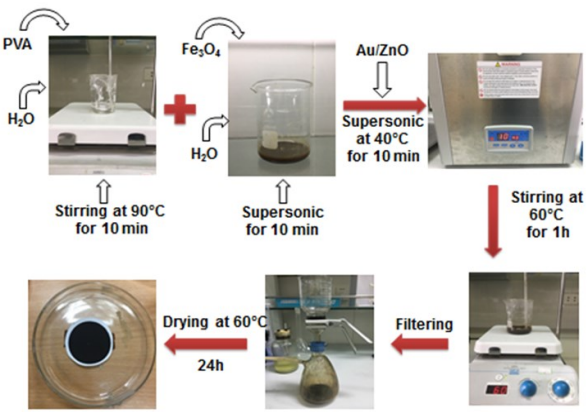

Figure 3. The synthesis procedure of AZF nanocomposites.

Copyright © 2023, ISSN 1978-2993

10 min. Then the Fe_3O_4 was added to PVA, and the suspension was mixed with 0.05 g Au/ZnO and sonicated for 5 min at 40 °C, heated at 60 °C, then stirred for 3 h. The precipitate was filtered, washed with distilled water several times, and finally dried in an oven at 60 °C for 1 day to obtain Au/ZnO/Fe_3O_4 nanocomposite, which was named AZF. The synthesis procedure is shown in Figure 3. To study the effect of the PVA content in composite on catalytic performance, the mass ratio of Fe_3O_4 and PVA were carried out at 1:2, 2:3, 1:1, 2:1, 4:1, and 5:1 corresponding to the PVA contents of 0.1, 0.075, 0.05, 0.025, 0.0125, and 0.01 g, respectively, at the same mass of Fe_3O_4 of 0.05 g.

2.6 Characterizations

The XRD pattern was analyzed by a Bruker D8 Advance diffractometer (Germany) with Cu Kα irradiation (40 kV, 40 mA) to investigate the crystalline phase of samples. The morphol-

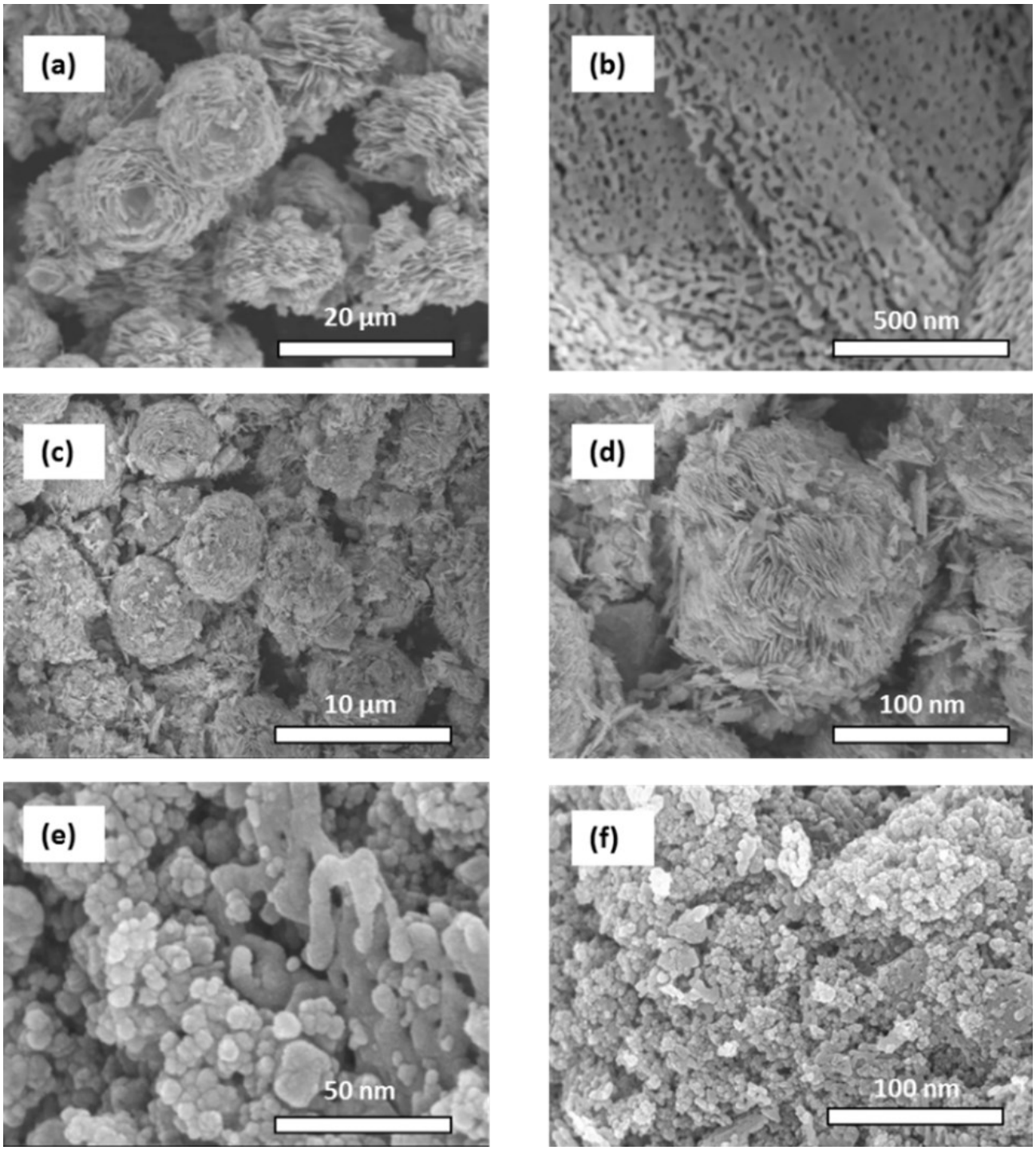

Figure 4. SEM images of (a-b) ZnO, (c-d) Au/ZnO, (e-f) AZF with different resolutions.

Copyright © 2023, ISSN 1978-2993

ogy and size of the samples were observed by transmission electron microscopy (TEM, JEM-2010), emission scanning electron microscopy (FE-SEM, JEOL-7600F) and energy dispersive X-ray spectroscopy (EDS, JEOL-7600F). The Fourier transform infrared spectra (FT-IR) were measured by infrared spectrometer (FT-IR, Madison, WI, USA).

2.7 Photocatalytic Test

The experiments were conducted by the batch reactor. A 250 mL glass beaker containing the concentration of TA of 5 mg/L, the catalyst dosage of 0.25 g/L was added into the beaker and sonicated for 5 min. The mixture was left in the dark for 30 min to achieve the adsorption/desorption equilibrium and then placed under the Hg lamp 250 W. At intervals, a little of the mixture from the beaker was filtered by a syringe filter (0.45 μm PTFE membrane) to extrude the catalyst. The concentration of dye was determined by the spectrophotometry method (UV-Vis, Agilent 8453 instrument). The important parameters of the catalysis process are calculated using the following equations:

$$\ln\left(\frac{C_0}{C_t}\right) = kt \quad (7)$$

$$Degradation\ efficiency\ (DE;\%) = \frac{C_0 - C_t}{C_0} \times 100 \quad (8)$$

$$Degradation\ capacity\ (DC;mg/g) = \frac{(C_0 - C_t) \times V}{m} \quad (9)$$

where, k is the pseudo-first-order rate constant, the k value was calculated from the slope of the ln (C_0/C_t) − t plots; C_0 and C_t are the concentrations of dye at initial (t = 0) and time t (min), respectively; V is the volume of dye solution (L) and m is the mass of the adsorbent (g).

3. Results and Discussion

3.1 Physicochemical Characterization

The morphology of the samples is presented in Figure 4. The ZnO was a hierarchical structure like a uniform flower with a size of ap-

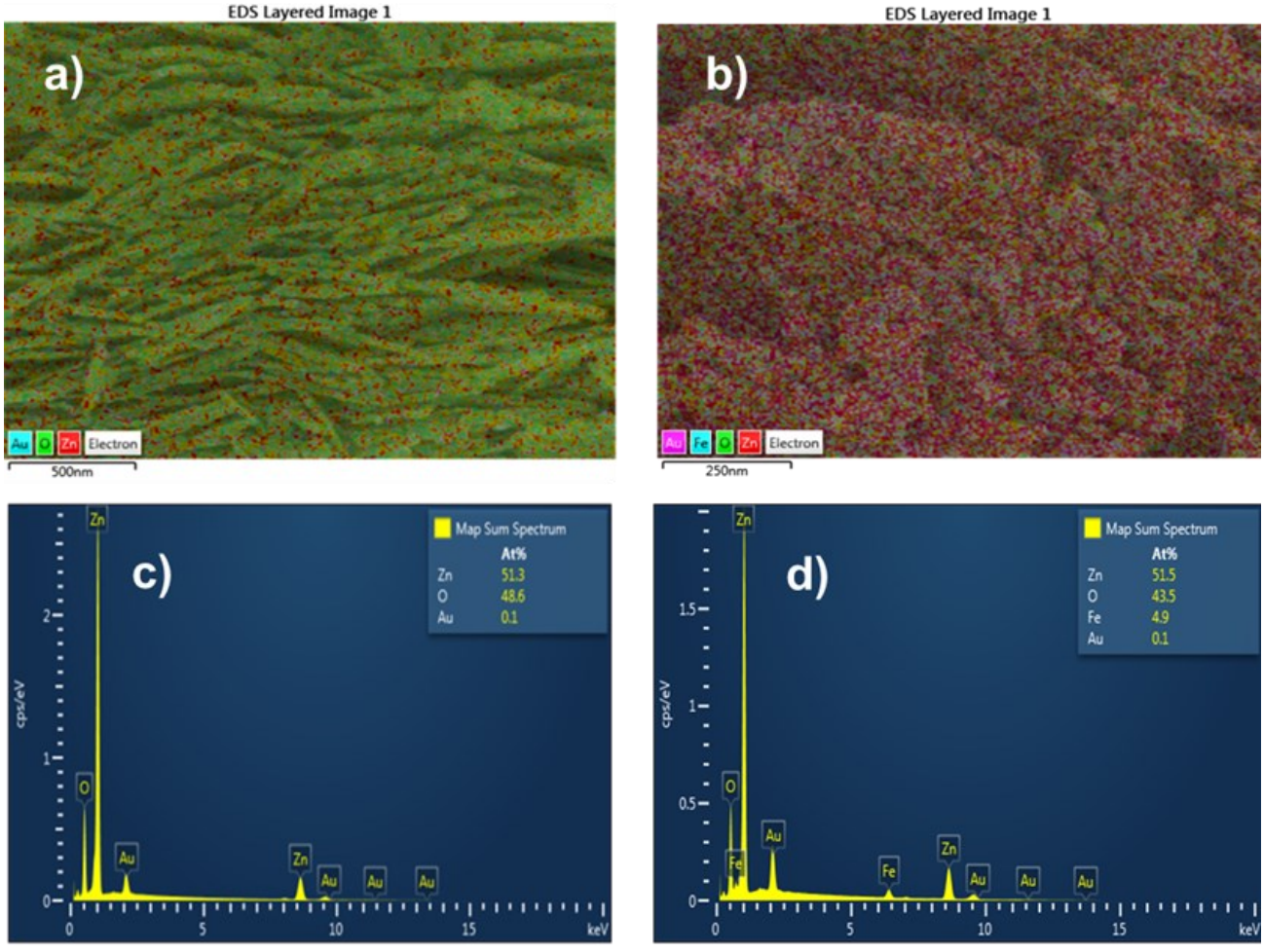

Figure 5. (a-b) EDS mapping images and (c-d) EDS spectra of Au/ZnO and AZF, respectively.

Copyright © 2023, ISSN 1978-2993

proximately 10-15 μm (Figure 4(a)). The ZnO microstructure was composed of many thin petals made of oxide particles, built from many holes of 20 nm (Figure 4(b)). The size and shape of the Au/ZnO composite were similar to bare ZnO, but the petals became denser due to the deposition of Au in composite, in Figure 4(c)-(d). The TEM results in the previous study showed that the size of ZnO particles was about 30-50 nm and that of Au particles was about 3-5 nm [13]. Meanwhile, Figure 4(e)-(f) showed that the structure of the AZF material had significantly changed from Au/ZnO, showing the appearance of spherical particles that tend to gather together into a cluster of particles. These particles were coupled and densely distributed on the surface of the material, making it more difficult to observe Fe_3O_4 composites. However, it played the role of creating magnetism to recover the material after the catalytic process using magnets.

Although Fe was not recognized in the SEM, the results of the EDS mapping image (Figure 5(a)-(b)) demonstrated the uniform dispersion of Au and Fe in the composite. It was further proven by EDS results, showing the element contents of 51.3, 48.6 and 0.1% for Zn, O, and Au, respectively, in Figure 5(c). And, the contents were 51.5, 43.5, 4.9 and 0.1 for Zn, O, Fe, and Au, respectively, in Figure 5(d).

The hexagonal wurtzite structure of ZnO was proved by the XRD results, in Figure 6. In which, the intense peaks at 2θ of 31.50, 34.12, 35.97, 47.28, 56.38, 62.62, 67.74, and 68.90° were assigned to the characteristic planes of (100), (002), (101), (102), (110), (103), (112) and (201), respectively, of ZnO crystallites [13]. The low intense peaks at 30.21, 37.13, 43.37, 53.81, 57.05, and 63.44° corresponding to (220), (222), (400), (422), (511), and (440) plans could be assigned to Fe_3O_4 crystallites [22]. The signal of Au was not detected in Au/ZnO composite, although it was recognized by EDS mapping and spectra (Figure 5). This was possibly assigned

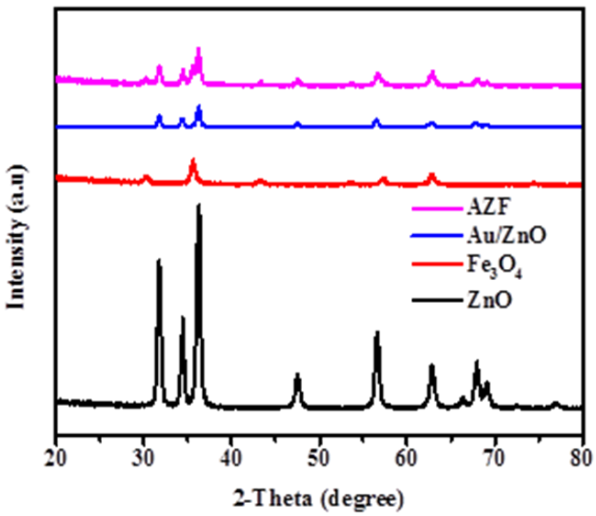

Figure 6. XRD patterns of ZnO, Fe_3O_4, Au/ZnO and AZF.

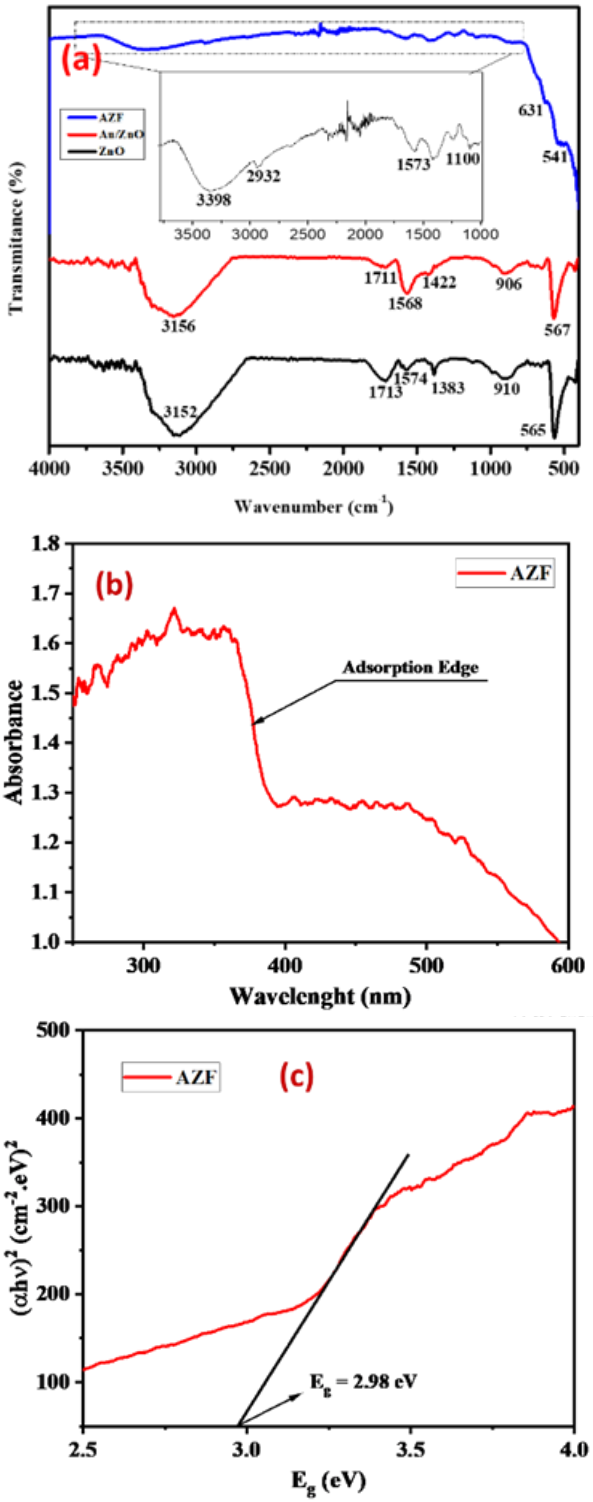

Figure 7. (a) FT-IR spectra of ZnO, Au/ZnO and AZF composite, (b) and (c) UV-Vis-DR and Tauc curve of the AZF sample, respectively.

Copyright © 2023, ISSN 1978-2993

to Au at a low content and small particle size [13]. Also, the XRD intensity of ZnO was noticeably reduced by adding Au into the composite. For the AZF composite, all the signals of ZnO, Au, and Fe_3O_4 appeared together with low intensity. Furthermore, no impurity peaks were detected, indicating the high purity of the composite.

The FT-IR spectra of samples are shown in Figure 7. The strong bands at 3152, 3156, and 3398 cm^{-1} in all samples were related to the presence of hydroxyl groups and attributed to O–H stretching vibration of absorbed water (H–O–H) [23]. The band observed at 2932 cm^{-1} might be attributed to valence oscillations of the C–H, and the band at 1100 cm^{-1} was attributed to valence vibration of the C–O bond of PVA in the AZF composite. The bands at 1574, 1568, and 1573 cm^{-1} of ZnO, Au/ZnO, and AZF might be attributed to the C=O bond [24]. The small band at 1713, 1383, and 910 cm^{-1} were associated with the vibration of the O–H bond of Zn–O–H [2]. When Au was added to the Au/ZnO composite, the adsorption was lowered, whereas the band at 1574 cm^{-1} was more intense. The characteristic absorption of the Fe–O bond of the crystalline lattice of Fe_3O_4 in the AZF composite was recognized at 541 and 631 cm^{-1} [25], while the strong bands at 567 and 565 cm^{-1} of ZnO and Au/ZnO composite were attributed to the Zn–O vibration in both samples [13].

The UV-Vis-DR analysis results shown in Figure 7(b) indicate that the AZF material had a strong ability to absorb radiation in the wavelength range of 250-400 nm. Besides, a 500 nm convex curve demonstrated the absorption capacity of AZF in the visible light region. According to calculation from Tauc method, E_g of AZF material was 2.98 eV. It was smaller than that of ZnO and Au/ZnO of 3.15 and 3.12 eV, respectively, in our previous study [13].

3.2 Degradation of Dyes

3.2.1 Effect of PVA content

Figure 8 shows the TA degradation efficiency of AZF composites with different PVA contents. Bare ZnO had DE and rate constant of 95.1% and 0.037 min^{-1}, respectively. With the addition of Au into ZnO, the rate of reaction and DE become higher, showing 98.6% and 0.057 min^{-1}, respectively. The DE and rate constant were 60.4% and 0.011 min^{-1} for the AZF-0.01. These achieved 71.9% and 0.014 min^{-1}, respectively, for the AZF-0.0125. However, at higher PVA content than 0.0125 g, the DEs and rate constants were 67.4, 60.1, 47.2, and 43.3 and 0.012, 0.005, 0.009, and 0.007 min^{-1} for AZF-0.025, AZF- 0.05, AZF-0.075, and AZF-0.1, respectively. PVA with fusible properties can dissolve well in solution at a temperature of 90 °C. Although PVA acts as the binder between Au/ZnO and Fe_3O_4, PVA can form a polymeric film, which is shown by the smooth surface in the FE-SEM results (Figure 4(e)-(f)), it prevents contact of the AZF catalyst with the solution. Besides, PVA can damage the flower-like structure of the Au/ZnO composite. These lead to a decrease in the catalytic decomposition of organic matter.

3.2.2 Fenton system catalyst

Hydroperoxide is a strong oxidizing agent, it can directly decompose persistent organic sub-

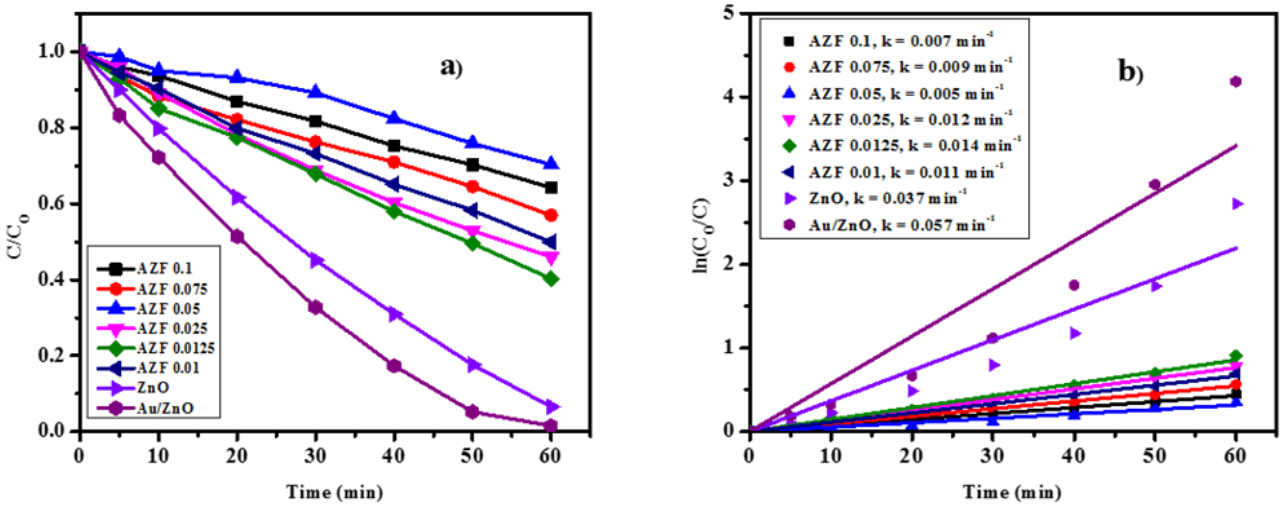

Figure 8. (a) Photocatalytic degradation of TA in ZnO, Au/ZnO, and AZF composites at the different PVA contents and (b) the kinetic curves. The reaction conditions: TA concentration of 10 mg/L, catalyst dosage of 0.5 g/L, and Hg lamp 250 W.

Copyright © 2023, ISSN 1978-2993

stances, but its reaction rate is relatively low without the initiator of the reaction. The Fenton catalyst system is possible with H_2O_2 and iron. In the presence of Fe^{2+} and Fe^{3+} ions, the generation of free radicals (•OH and $•O_2^-$) takes place rapidly, leading to an increase in the decomposition rate of organic matter in the solution. However, the Fenton process is strongly dependent on the pH of the solution, it is mainly due to the formation factors between iron and H_2O_2. The optimal pH for the conventional Fenton system was found to be around 3.0, regardless of the target substrate [26–29].

The AZF and Fe_3O_4 samples were used to conduct experiments at fixed reaction conditions (catalyst dosage of 0.5 g/L, TA concentration of 10 mg/L, pH of 3.0, H_2O_2 concentration of 12 mM). The results are presented in Figure 9. With the AZF sample without H_2O_2, the removal efficiency of TA was 42.0%, which could be attributed to the adsorption of TA on the material. With the presence of H_2O_2, the DE of the Fenton catalyst with AZF was only 30.3%, meanwhile, the reaction in the dark gave the DE of 19.6%. The catalyst performance was highest for Fe_3O_4 showing a DE of 97.1 % in the initial 10 min. The low degradation efficiency of AZF–H_2O_2 could be explained because as following reasons: (1) The PVA is completely dissolved and dispersed on the Fe_3O_4 particles, which carry the Au/ZnO, however, this prevents the contact of the catalyst with the solution, leading to a decrease in the efficiency of the Fenton process. (2) In addition, at a relatively acidic pH = 3, ZnO can react with acids to produce the corresponding salt in Equation (10). As a result, the catalytic efficiency is reduced.

$$ZnO_{(s)} + 2H^+_{(aq)} \rightarrow Zn^{2+}_{(aq)} + H_2O \quad (10)$$

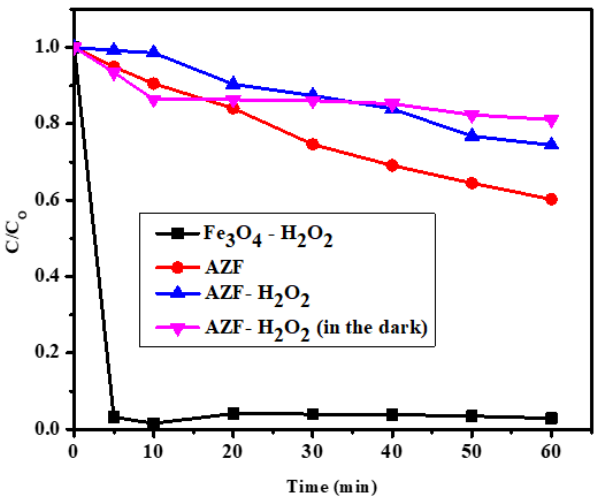

Figure 9. Fenton process on samples, the reaction conditions (catalyst dosage of 0.5 g/L, TA concentration of 10 mg/L, pH of 3.0, H_2O_2 concentration of 12 mM).

3.2.3 Effect of the pH on the degradation of TA

Experiments were carried out at the pH range of 3.0 – 11.0 at fixed conditions (catalyst dosage of 0.5 g/L, H_2O_2 concentration of 12 mM, TA concentration of 10 mg/L, and light irradiation of Hg lamp 250 W). The results are shown in Figure 10. The degradation of TA was different with solution pH. The reaction of TA in AZF - H_2O_2 composite at the pH of 3.0 was relatively low. When the pH value increased to 5.0, the degradation efficiency and reaction rate sharply increased, these approached 81.5 % and 0.020 min^{-1}, respectively. At higher pH,

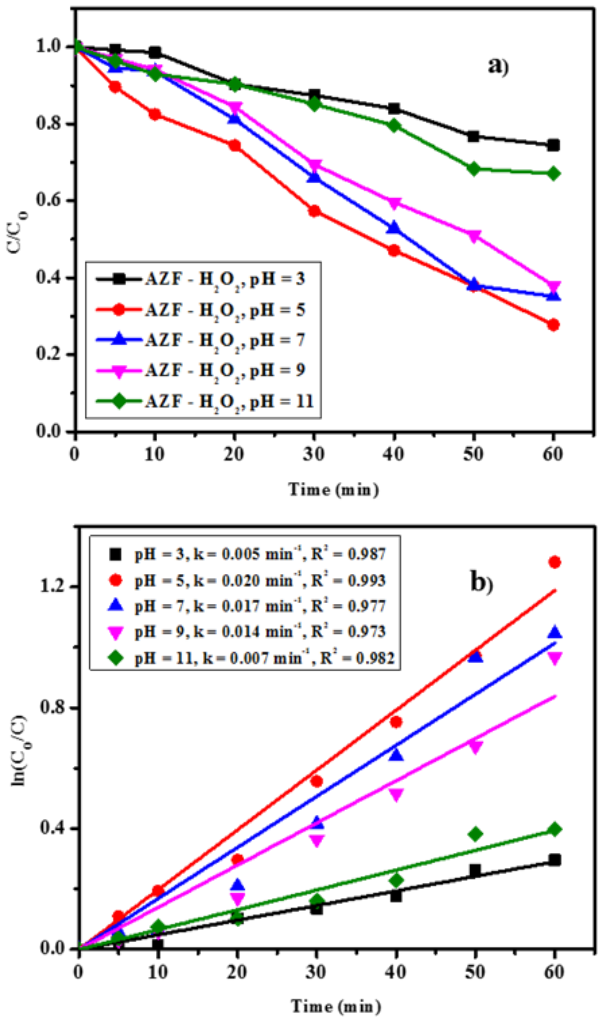

Figure 10. (a) Effect of solution pH on photodegradation TA of AZF – H_2O_2, (b) the kinetic curves. The reaction conditions: Catalyst dosage of 0.5 g/L, TA concentration of 10 mg/L, H_2O_2 concentration of 12 mM, pH of 5.0, and Hg lamp 250 W.

Copyright © 2023, ISSN 1978-2993

the reaction was decreased with pH. The DE and reaction constant were 76.0% and 0.017 min^{-1}, respectively, at the pH of 7.0. These were decreased to 37.9% and 0.007 min^{-1}, respectively, at the pH of 11.0, in Figure 10.

The low reaction rates at a strong acidic or strongly alkaline medium can be assigned to the dissolution of ZnO [30], since ZnO is amphoteric oxide. At low pH, ZnO can react with acids to produce the corresponding salt. At high pH, ZnO can react with bases to form complexes $[Zn(OH)_4]^{2-}$. Moreover, at high pH, the formation of relatively inactive iron oxyhydroxides and ferric hydroxide precipitate [31] leads the fewer •OH radicals being generated. Therefore, the oxidizing capacity of the catalyst is decreased with increasing pH. In addition, the oxidation potential of the redox pair •OH/H_2O was reduced with an increase in pH, which is 2.59V versus normal hydrogen electrode (NHE) at the pH of 0 and 1.64 V at the pH of 14 [32]. Furthermore, at high pH, the decomposition of H_2O_2 increased, in Equation (11) [33]. As a result, the reaction efficiency of the AZF–H_2O_2 for degrading organic compounds is reduced at both high and low pH. In this study, the pH of 5.0 was found to be the most efficient condition for the AZF-0.0125 catalyst in the presence of H_2O_2. This could be due to at the right pH environment, the addition of H_2O_2 not only stimulates the Fenton reaction but also can accelerate the generation of •OH radicals from either scavenging e_{CB}^- on surface AZF catalyst or absorbing the photon energy, leading to an enhanced degradation process of organic matters [13].

$$2H_2O_2 \rightarrow O_2 + 2H_2O \quad (11)$$

3.2.4 Effect of oxidizing agents

To study the effects of oxidizing agents on the photocatalytic performance of AZF composite, the H_2O_2 and O_2 were used while other conditions were fixed at catalyst dosage of 0.5 g/L, TA concentration of 10 mg/L, H_2O_2 concentration of 12 mM, O_2 bubble of 5 mL/min, pH of 5.0, and Hg lamp 250 W. The results are presented in Figure 11. Photocatalysis mainly occurred with AZF in the presence of visible light irradiation. However, the reaction of AZF slightly increased with the presence of H_2O_2, showing the DE, rate constant, and degradation capacity of 74.5%, 0.016 min^{-1}, and 14.9 mg/g, respectively. Since hydrogen peroxide acts as an electron acceptor, it can promote charge separation and production of •OH radicals according to Equations (12)–(14). And, these reactions can enhance the catalytic ability of the composite because of the formation of additional oxidizing species and prevent electron-hole recombination.

$$e_{CB}^- + H_2O_2 \rightarrow \cdot OH + OH^- \quad (12)$$
$$H_2O_2 + \cdot O_2 \rightarrow \cdot OH + OH^- + O_2 \quad (13)$$
$$H_2O_2 + h\nu \rightarrow 2 \cdot OH \quad (14)$$

According to previous research, the presence of O_2 improved the catalytic ability of the Au/ZnO composite [13]. However, in this study, when O_2 was added to the AZF composite, the red-brown $Fe(OH)_3$ precipitate appeared at the high pH the solution, in Equation (15), which is insoluble in solution. It reduces the concentration of Fe^{3+} ions and also reduces the light transmission in the solution due to an increase in the density of precipitated particles. As a re-

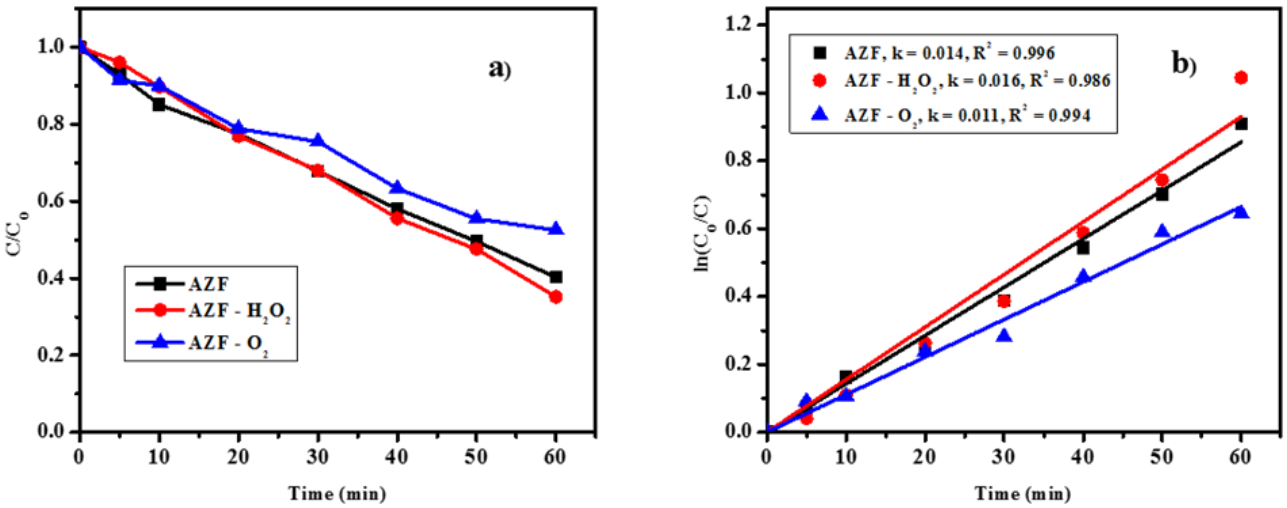

Figure 11. (a) Effect of oxidizing agent on degradation of TA and (b) the kinetic curves. The reaction conditions: Catalyst dosage of 0.5 g/L, TA concentration of 10 mg/L, pH of 5.0, H_2O_2 concentration of 12 mM, O_2 bubble of 5 mL/min, and Hg lamp 250 W.

Copyright © 2023, ISSN 1978-2993

sult, the catalytic activity of the AZF with adding O_2 was lower than that of adding H_2O_2. The performance of the catalyst was reduced, showing the DE and reaction constant, and degradation capacity of 58.6%, 0.011 min^{-1}, and 11.7 mg/g, respectively.

$$4Fe_3O_4 + 18H_2O + O_2 \rightarrow 12Fe(OH)_3 \qquad (15)$$

3.3 Reusability of Catalyst

The reusability test of the AZF 0.0125M sample was evaluated in consecutive cycles. After an experiment, the catalyst was collected with a magnet, in Figure 12(a), then filtered and washed with distilled water and ethanol several times, dried at 60 °C for 24 h, and then re-used for the next experiment. The results are presented in Figure 12(b), the DE of tartrazine under Hg lamp 250W in the first experiment was 81.5%, The catalytic efficiency was relatively decreased in the 2nd cyclic experiment, exhibiting the DE of 61.1%. The element analysis results showed that the contents of Zn, Fe, and Au of the AZF sample before the reaction were 50.4, 6.1, and 0.12%, respectively, and those of the sample after 2 cycles were 47.2, 6.1, and 0.12%, respectively. This implied a slight release of ZnO after the catalytic processes. The SEM result of the AZF after 2 cycles indicated that the particles tend to aggregate after the regenerations, in Figure 12(c). Besides, the intensity of XRD peaks of the AZF sample after 2 cycles gradually decreased, indicating that the crystallinity of the composite was reduced after the reaction processes. All of these caused a slight decrease in the efficiency of the AZF catalyst after the reuse processes. However, the catalytic efficiency also tended to be stable after the first regeneration, and the material included both photocatalytic and the Fenton catalytic processes, the catalyst had a good physical stability. Therefore, AZF composite can be a considerable choice to treat pollutants in wastewater and have the potential for practical applications in industries.

3.4 Proposed Reaction Mechanism

Figure 13 shows the photocatalytic and Fenton mechanism of degradation of dye on AZF. When ZnO is photo-induced by visible light with photonic energy equal to or greater than the excitation energy (E_g), e^- from the valence

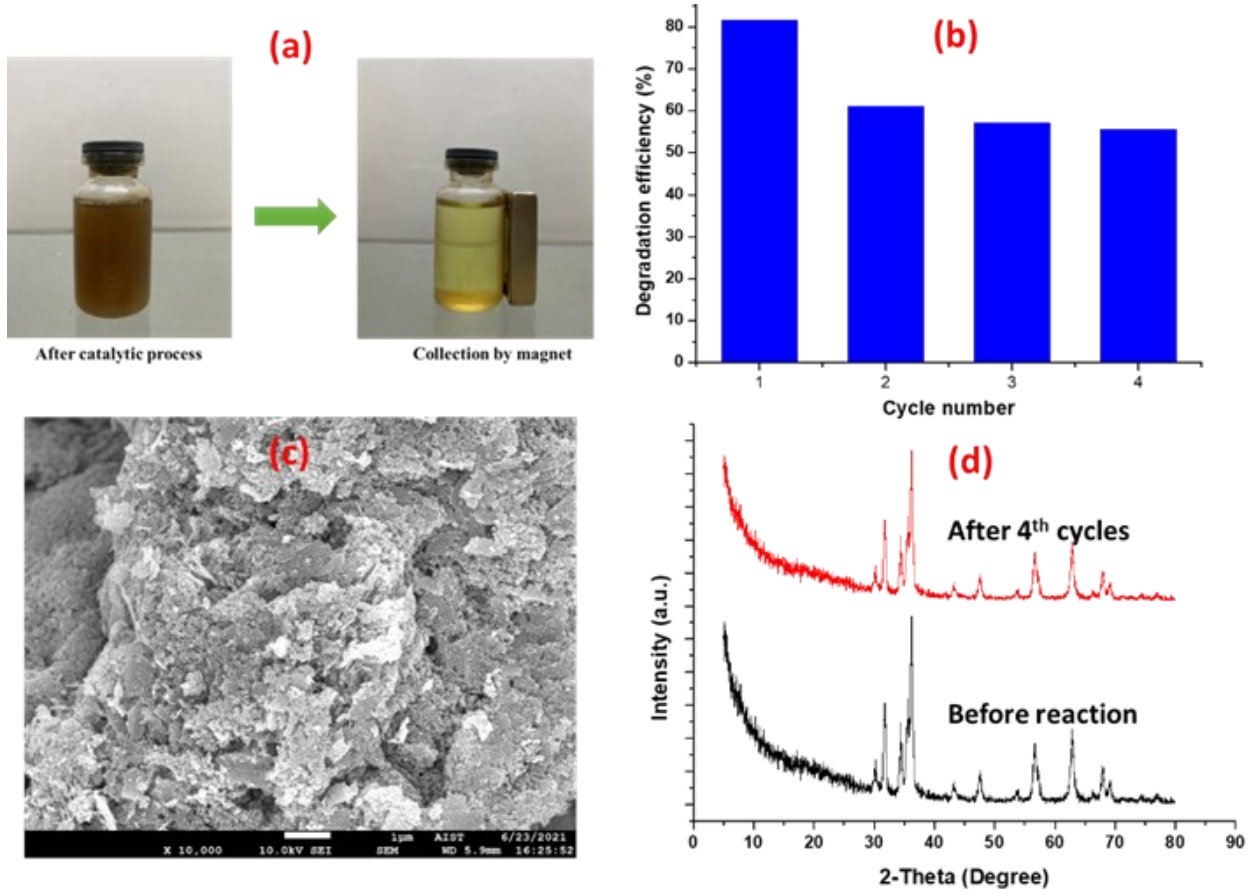

Figure 12. (a) The recover the catalyst by magnet, (b) reusability test of AZF, (c) SEM image of AZF after 2 cycles, and (d) XRD patterns of AZF before reaction and after 2 cycles.

Copyright © 2023, ISSN 1978-2993

band (VB) is promoted to an empty conduction band (CB) [34]. This photo-induced process produces electron-hole pairs (e^- and h^+) and carries an electrical charge, which can interact with oxygen and water at the surface of ZnO to produce oxidizing agents including H_2O_2, $\cdot O_2^-$, and $\cdot OH$. Two agents are formed $\cdot O_2^-$, $\cdot OH$ will interact with organic substances and decompose them into CO_2 and H_2O. However, the rapid recombination rate of electrons and holes causes a decrease in the photodegradation reaction. Additionally, it has also been noted that the solar energy conversion performance of ZnO is affected by its optical absorption ability, which has been associated with its large band gap energy. Therefore, intense efforts have been made to improve the optical properties of ZnO by minimizing the band gap energy and inhibiting the recombination of electrons and holes [34].

If Au nanoparticles are presented in the composite, an energy barrier, the Schottky barrier, is formed between Au and ZnO, which prevents the direct transition of electrons from the conduction band to holes of ZnO. While electrons will be transferred from the conduction band of ZnO to the Au nanoparticles depicted by the red arrow. As a result, the electrons on Au can interact with O_2 to generate $\cdot O_2^-$ radicals, and the holes in ZnO can interact with $H_2O_2/H_2O_2/OH^-$ to generate $\cdot OH$ radicals [13]. The main role of Fe_3O_4 is as a magnet to recover the material after catalysis. These processes are described by the following Equations (16)–(25).

$$ZnO + h\nu \rightarrow ZnO\ (e^- + h^+) \quad (16)$$
$$e^- + O_2 \rightarrow \cdot O_2^- \quad (17)$$
$$\cdot O_2^- + H^+ \rightarrow HO_2 \quad (18)$$
$$HO_2\cdot + HO_2\cdot \rightarrow H_2O_2 + O_2 \quad (19)$$
$$H_2O_2 + h\nu \rightarrow 2\ \cdot OH \quad (20)$$
$$ZnO\ (e^-) + Au \rightarrow ZnO + Au\ (e^-) \quad (21)$$
$$Au\ (e^-) + O_2 \rightarrow \cdot O_2^- + Au \quad (22)$$
$$ZnO\ (h^+) + H_2O \rightarrow ZnO + H^+ + \cdot OH \quad (23)$$
$$(\cdot O_2^- + \cdot OH) + \text{organic dyes} \rightarrow \text{Intermediate products} \quad (24)$$
$$(\cdot O_2^- + \cdot OH) + \text{Intermediate products} \rightarrow CO_2 + H_2O \quad (25)$$

When H_2O_2 is added into catalyst system, it forms a Fenton catalyst system, in Figure 13(b). The traditionally accepted Fenton mechanism is represented by Equations (26)–(34):

$$Fe^{2+} + H_2O_2 \rightarrow Fe^{3+} + OH^- + \cdot OH \quad (26)$$
$$Fe^{3+} + H_2O_2 \rightarrow Fe^{2+} + HO_2\cdot + H^+ \quad (27)$$
$$Fe^{2+} + \cdot OH \rightarrow Fe^{3+} + OH^- \quad (28)$$
$$Fe^{2+} + HO_2\cdot \rightarrow Fe^{3+} + HO_2^- \quad (29)$$
$$Fe^{3+} + HO_2\cdot \rightarrow Fe^{2+} + O_2 + H^+ \quad (30)$$
$$\cdot OH + \cdot OH \rightarrow H_2O_2 \quad (31)$$
$$\cdot OH + H_2O_2 \rightarrow HO_2\cdot + H_2O \quad (32)$$
$$HO_2\cdot + HO_2\cdot \rightarrow H_2O_2 + O_2 \quad (33)$$
$$\cdot OH + HO_2\cdot \rightarrow O_2 + H_2O \quad (34)$$

Equation (26) is recognized as the Fenton reaction and implies the oxidation of ferrous to ferric ions to decompose H_2O_2 into hydroxyl radicals. It is usually considered the core of Fenton chemistry. The generated ferric ions can be reduced by reaction with excess hydrogen peroxide to form again ferrous ions and more radicals as shown in Equation (27). This reaction is called a Fenton-like reaction and slower than Fenton reaction, and allows Fe^{2+} regeneration in an effective cyclic mechanism. In a Fenton-like reaction, apart from ferrous ion regeneration, hydroperoxyl radicals ($HO_2\cdot$) are produced. Hydroperoxyl radicals may also

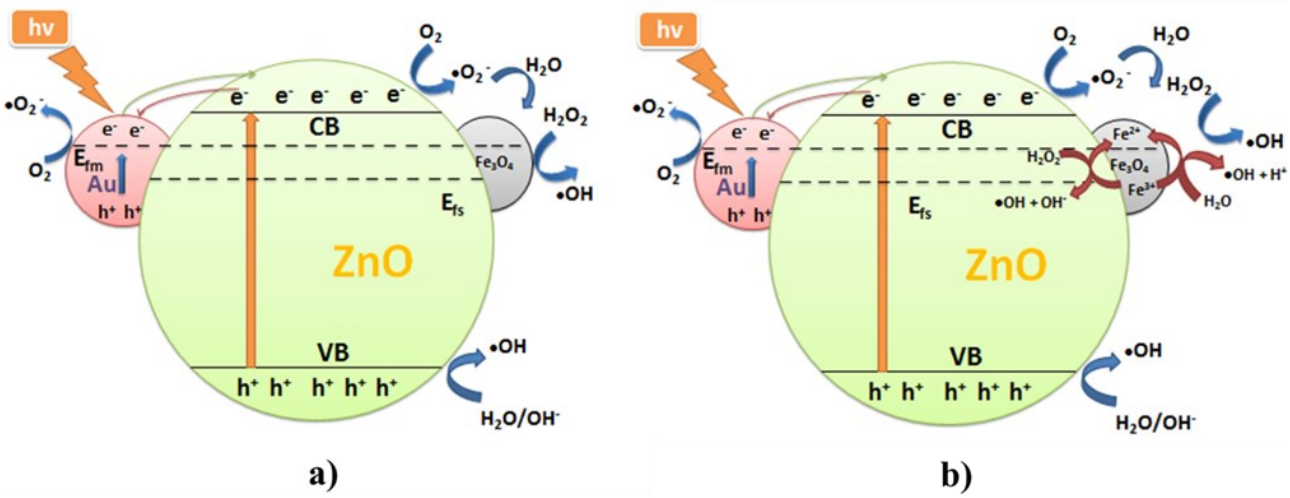

Figure 13. Schematic model for the photocatalytic mechanism of (a) Au/ZnO/Fe_3O_4 composite, (b) Au/ZnO/Fe_3O_4 composite with H_2O_2.

Copyright © 2023, ISSN 1978-2993

attack organic contaminants, but they are less sensitive than hydroxyl radicals. Equations (32)–(34) also reported to occur during the Fenton process and they are radical–radical reactions or hydrogen peroxide–radical reactions [34]. Hydroxyl radicals may attack organic radicals produced by organics present in wastewater. Those radicals form dimmers or react with ferrous and ferric ions, as shown in Equations (35)–(37) [35,36]. Thus, when adding H_2O_2 to the AZF catalyst, Fe_3O_4 not only plays the role of catalytic recovery but also contributes to the generation of •OH radicals that degrade organic dyes. However, the Fenton catalyst system at a pH of 6 is an optimal condition, near neutral pH will give the best photocatalytic efficiency and Fenton reaction.

$$2R\bullet \rightarrow RR \quad (35)$$

$$R\bullet + Fe^{2+} \rightarrow R^- + Fe^{3+} \quad (36)$$

$$R + Fe^{3+} \rightarrow R^+ + Fe^{2+} \quad (37)$$

4. Conclusion

ZnO based-composites were successfully prepared via a simple mixing method. The ZnO microstructure was composed of many thin petals made of oxide nanoparticles with sizes of 30-50 nm, building many holes of 20 nm. The size and shape of the Au/ZnO composite were similar to bare ZnO, but the petals became denser due to the deposition of Au in the composite. The structure of the AZF composite had significantly changed from Au/ZnO, showing the appearance of spherical particles that tend to gather together into a cluster of particles.

The AZF-0.0125 sample exhibited the highest performance among samples with the PVA contents from 0.01 to 0.1 g, showing the DE and rate constant were 71.9% 0.014 min^{-1}, respectively. The reduction of catalytic activity of the AZF composite compared to ZnO and Au/ZnO could be explained by the formation of a film that prevents contact of the catalyst with the solution of PVA. At the pH of 3.0, in the presence of H_2O_2, Fe_3O_4 exhibited a strong Fenton system for the degradation of TA. However, when Fe_3O_4 was mixed with Au/ZnO by a binder PVA to form Au/ZnO/Fe_3O_4 composite, the optimal pH for the catalytic reaction was 5.0, showing the DE and rate constant of 81.5% and 0.020 min^{-1}, respectively. The presence of H_2O_2 accelerated the generation of •OH radicals, leading to improve degradation of TA. However, in this study, when O_2 was added to the AZF composite, the red-brown $Fe(OH)_3$ precipitate appeared in the high pH solution, which is insoluble in solution. It reduces the concentration of Fe^{3+} ions and also reduces the light transmission in the solution due to an increase in the density of precipitated particle. Although the catalytic efficiency of the composite was decreased significantly after 2 cycles, it was stable in subsequent cycles. Besides, at the reaction conditions of pH = 5.0, catalyst dosage = 0.5 g/L, H_2O_2 concentration = 12 mM, and under Hg, the composite still gave relatively high photocatalytic efficiency. Furthermore, the composites had mechanical and chemical stabilities. Therefore, the AZF composite can be a considerable choice to treat pollutants in wastewater and will have the potential for practical applications in industries.

Acknowledgments

The authors are grateful for the financial support from Vietnamese Ministry of Education and Training under grant number CT2022.04.BKA.01.

CRediT Author Statement

Author Contributions: Linh Vo Quang: Methodology, Investigation, Resources, Experiment and Writing; Anh-Tuan Vu: Review, Editing, and Validation. All authors have read and agreed to the published version of the manuscript.

References

[1] Liu, L., Bilal, M., Duan, X., Iqbal, H.M.N. (2019). Mitigation of environmental pollution by genetically engineered bacteria - Current challenges and future perspectives. *Science of The Total Environment,* 667, 444-454. DOI: 10.1016/j.scitotenv.2019.02.390.

[2] Mai, L.T., Hoai, L.T., Tuan, V.A. (2018). Effects of reaction parameters on photodegradation of caffeine over hierarchical flower-like ZnO nanostructure. *Vietnam Journal of Chemistry*, 56(5), 647-653. DOI: 10.1002/vjch.201800064.

[3] Vu, A.T., Pham, T.A.T., Mac, V.H., Nguyen, T.H. (2021). Facile Controlling of the Physical Properties of Zinc Oxide and Its Application to Enhanced Photocatalysis. *Journal of Analytical Methods in Chemistry,* 2021, 5533734. DOI: 10.1155/2021/5533734.

[4] Nguyen Thi, T.A., Vu, A.-T. (2022). Nanocomposite ZnO/g-C_3N_4 for Improved Degradation of Dyes under Visible Light: Facile Preparation, Characterization, and Performance Investigations. *Bulletin of Chemical Reaction Engineering & Catalysis*, 17(2), 403-419. DOI: 10.9767/bcrec.17.2.13931.403-419.

Copyright © 2023, ISSN 1978-2993

[5] Mac, V.H., Vu, A.-T. (2022). Controlling the 3D flower-like ZnO via simple precipitation method and its formation mechanism and photocatalytic application. Journal *of the Chinese Chemical Society*, 69(12), 1997-2005. DOI: 10.1002/jccs.202200437.

[6] Nguyen, T.H., Vu, A.-T. (2022). Preparation of B/ZnO Nanocomposite by Simple Mechanical Combustion Method for Removal of Antibiotics in Aqueous Environments. *Bulletin of Chemical Reaction Engineering & Catalysis*, 17(4), 786-797. DOI: 10.9767/bcrec.17.4.16090.786-797.

[7] Andrade, G.R.S., Nascimento, C.C., Silva Júnior, E.C., Mendes, D.T.S.L., Gimenez, I.F. (2017). ZnO/Au nanocatalysts for enhanced decolorization of an azo dye under solar, UV-A and dark conditions. *Journal of Alloys and Compounds,* 710, 557-566. DOI: 10.1016/j.jallcom.2017.03.295.

[8] Cheng, Y.-F., Jiao, W., Li, Q., Zhang, Y., Li, S., Li, D., Che, R. (2018). Two hybrid Au-ZnO aggregates with different hierarchical structures: A comparable study in photocatalysis. *Journal of Colloid and Interface Science*, 509, 58-67. DOI: 10.1016/j.jcis.2017.08.077.

[9] Li, C., Lin, Y., Li, F., Zhu, L., Meng, F., Sun, D., Zhou, J., Ruan, S. (2015). Synthesis and highly enhanced acetylene sensing properties of Au nanoparticle-decorated hexagonal ZnO nanorings. *RSC Advances*, 5, 87132-87138. DOI: 10.1039/C5RA16552K.

[10] Ren, C., Yang, B., Wu, M., Xu, J., Fu, Z., lv, Y., Guo, T., Zhao, Y., Zhu, C. (2010). Synthesis of Ag/ZnO nanorods array with enhanced photocatalytic performance. *Journal of Hazardous Materials*, 182(1), 123-129. DOI: 10.1016/j.jhazmat.2010.05.141.

[11] Verma, S., Tirumala Rao, B., Jayabalan, J., Rai, S.K., Phase, D.M., Srivastava, A.K., Kaul, R. (2019). Studies on growth of Au cube-ZnO core-shell nanoparticles for photocatalytic degradation of methylene blue and methyl orange dyes in aqueous media and in presence of different scavengers. *Journal of Environmental Chemical Engineering*, 7(4), 103209. DOI: 10.1016/j.jece.2019.103209.

[12] Vu, A.-T., Tuyet Pham, T.A., Tran, T.T., Nguyen, X.T., Tran, T.Q., Tran, Q.T., Nguyen, T.N., Doan, T.V., Vi, T.D., Nguyen, C.L., Nguyen, M.V., Lee, C.-H. (2020). Synthesis of Nano-Flakes Ag•ZnO•Activated Carbon Composite from Rice Husk as A Photocatalyst under Solar Light. *Bulletin of Chemical Reaction Engineering & Catalysis*, 15(1), 264-279. DOI: 10.9767/bcrec.15.1.5892.264-279.

[13] Vu, A.-T., Pham, T.A.T., Do, X.T., Tran, V.A., Le, V.D., Truong, D.D., Nguyen, T.H., Nguyen, M.V. (2021). Preparation of Hierarchical Structure Au/ZnO Composite for Enhanced Photocatalytic Performance: Characterization, Effects of Reaction Parameters, and Oxidizing Agent Investigations. *Adsorption Science & Technology*, 2021, 5201497. DOI: 10.1155/2021/5201497.

[14] Pham, T.A.T., Tran, V.A., Le, V.D., Nguyen, M.V., Truong, D.D., Do, X.T., Vu, A.-T. (2020). Facile Preparation of ZnO Nanoparticles and Ag/ZnO Nanocomposite and Their Photocatalytic Activities under Visible Light. *International Journal of Photoenergy*, 2020, 8897667. DOI: 10.1155/2020/8897667.

[15] Liu, H., Feng, J., Jie, W. (2017). A review of noble metal (Pd, Ag, Pt, Au)–zinc oxide nanocomposites: synthesis, structures and applications. *Journal of Materials Science: Materials in Electronics*, 28, 16585–16597. DOI: 10.1007/s10854-017-7612-0.

[16] Lu, A.-H., Salabas, E.L., Schüth, F. (2007). Magnetic Nanoparticles: Synthesis, Protection, Functionalization, and Application. *Angewandte Chemie*, 46(8), 1222-1244. DOI: 10.1002/anie.200602866.

[17] Costa, V.V., Jacinto, M.J., Rossi, L.M., Landers, R., Gusevskaya, E.V. (2011). Aerobic oxidation of monoterpenic alcohols catalyzed by ruthenium hydroxide supported on silica-coated magnetic nanoparticles, *Journal of Catalysis*, 282(1), 209-214. DOI: 10.1016/j.jcat.2011.06.014.

[18] Khoobi, M., Ma'mani, L., Rezazadeh, F., Zareie, Z., Foroumadi, A., Ramazani, A., Shafiee, A. (2012). One-pot synthesis of 4H-benzo[b]pyrans and dihydropyrano[c]chromenes using inorganic–organic hybrid magnetic nanocatalyst in water. *Journal of Molecular Catalysis A: Chemical*, 359 74-80. DOI: 10.1016/j.molcata.2012.03.023.

[19] Kiasat, A.R., Nazari, S. (2012). Magnetic nanoparticles grafted with ß-cyclodextrin–polyurethane polymer as a novel nanomagnetic polymer brush catalyst for nucleophilic substitution reactions of benzyl halides in water. *Journal of Molecular Catalysis A: Chemical*, 365, 80-86. DOI: 10.1016/j.molcata.2012.08.012.

[20] Zhang, L., Wang, Z., Xu, C., Li, Y., Gao, J., Wang, W., Liu, Y. (2011). High strength graphene oxide/polyvinyl alcohol composite hydrogels. *Journal of Materials Chemistry*, 21(28), 10399-10406. DOI: 10.1039/C0JM04043F.

Copyright © 2023, ISSN 1978-2993

[21] Wang, N., Chang, P.R., Zheng, P., Ma, X. (2014). Graphene–poly(vinyl alcohol) composites: Fabrication, adsorption and electrochemical properties. *Applied Surface Science*, 314, 815-821. DOI: 10.1016/j.apsusc.2014.07.075.

[22] Ngoc, K.H.P., Vu, A.-T. (2022). Simple Preparation of the $CuO \cdot Fe_3O_4$/Silica Composite from Rice Husk for Enhancing Fenton-Like Catalytic Degradation of Tartrazine in a Wide pH Range. *Adsorption Science & Technology*, 2022, 6454354. DOI: 10.1155/2022/6454354.

[23] Vu, A.-T., Xuan, T.N., Lee, C.-H. (2019). Preparation of mesoporous Fe_2O_3-SiO_2 composite from rice husk as an efficient heterogeneous Fenton-like catalyst for degradation of organic dyes. *Journal of Water Process Engineering*, 28, 169-180. DOI: 10.1016/j.jwpe.2019.01.019.

[24] Park, J.H., Choppala, G., Lee, S.J., Bolan, N., Chung, J.W., Edraki, M. (2013). Comparative Sorption of Pb and Cd by Biochars and Its Implication for Metal Immobilization in Soils. *Water, Air, & Soil Pollution*, 224(12), 1711. DOI: 10.1007/s11270-013-1711-1.

[25] Bordbar, A.K., Rastegari, A.A., Amiri, R., Ranjbakhsh, E., Abbasi, M., Khosropour, A.R. (2014). Characterization of Modified Magnetite Nanoparticles for Albumin Immobilization. *Biotechnology Research International*, 2014, 705068. DOI: 10.1155/2014/705068.

[26] Babuponnusami, A., Muthukumar, K. (2011). Degradation of Phenol in Aqueous Solution by Fenton, Sono-Fenton and Sono-photo-Fenton Methods. *Clean-soil, Air, Water*, 39(2) 142-147. DOI: 10.1002/clen.201000072.

[27] Eisenhauer, H.R. (1964). Oxidation of Phenolic Wastes. *Journal (Water Pollution Control Federation)*, 36(9), 1116-1128.

[28] Ma, Y.-S., Huang, S.-T., Lin, J.-G. (2000). Degradation of 4-nitrophenol using the Fenton process. *Water Science and Technology*, 42(3-4), 155-160. DOI: 10.2166/wst.2000.0373.

[29] Rivas, F.J., Beltrán, F.J., Frades, J., Buxeda, P. (2001). Oxidation of p-hydroxybenzoic acid by Fenton's reagent. *Water Research*, 35(2), 387-396. DOI: 10.1016/S0043-1354(00)00285-2.

[30] Spathis, P., Poulios, I. (1995). The corrosion and photocorrosion of zinc and zinc oxide coatings. *Corrosion Science*, 37(5), 673-680. DOI: 10.1016/0010-938X(95)80001-8.

[31] Parsons, S. (2004). *Advanced oxidation processes for water and wastewater treatment*. London: IWA publishing. DOI: 10.2166/9781780403076.

[32] Bossmann, S.H., Oliveros, E., Göb, S., Siegwart, S., Dahlen, E.P., Payawan, L., Straub, M., Wörner, M., Braun, A.M. (1998). New Evidence against Hydroxyl Radicals as Reactive Intermediates in the Thermal and Photochemically Enhanced Fenton Reactions. *The Journal of Physical Chemistry A*, 102(28), 5542-5550. DOI: 10.1021/jp980129j.

[33] Szpyrkowicz, L., Juzzolino, C., Kaul, S.N. (2001). A Comparative study on oxidation of disperse dyes by electrochemical process, ozone, hypochlorite and fenton reagent. *Water Research*, 35(9), 2129-2136. DOI: 10.1016/S0043-1354(00)00487-5.

[34] Ong, C.B., Ng, L.Y., Mohammad, A.W. (2018). A review of ZnO nanoparticles as solar photocatalysts: Synthesis, mechanisms and applications. *Renewable and Sustainable Energy Reviews*, 81, 536-551. DOI: 10.1016/j.rser.2017.08.020.

[35] Neyens, E., Baeyens, J. (2003). A review of classic Fenton's peroxidation as an advanced oxidation technique. *Journal of Hazardous Materials*, 98(1), 33-50. DOI: 10.1016/S0304-3894(02)00282-0.

[36] Pignatello, J.J., Oliveros, E., MacKay, A. (2006). Advanced Oxidation Processes for Organic Contaminant Destruction Based on the Fenton Reaction and Related Chemistry. *Critical Reviews in Environmental Science and Technology*, 36(1), 1-84. DOI: 10.1080/10643380500326564.

Copyright © 2023, ISSN 1978-2993